Optimal External Support Structure Design in Additive Manufacturing

Yu-Hsin Kuo[(✉)] and Chih-Chun Cheng

Department of Mechanical Engineering, Advanced Institute of Manufacturing
with High-tech Innovations, National Chung Cheng University,
Chia-yi, Taiwan (R.O.C.)
{d04420003,imeccc}@ccu.edu.tw

Abstract. A series of strategies for designing support structure to fabricate overhanging features in additive manufacturing (AM) is proposed. The focus of this study is to maximize the external support stiffness while requiring supports that can be easily removed, minimizing the time required to add the supports, and using the least amount of material. These design requirements become necessities not only for adding supports to improve processing and post-processing efficiency, but also for reducing the cost of supports while maintaining specimen geometry. A repulsion index (RI) is proposed for satisfying the easy removal requirement and minimizing the size of artifacts left on the specimen surface; a weighting function is applied to quantify the time consumption to build the supports. The proposed RI and cost due to additional material and time consumption in adding the support are formulated within a multi-objective topological optimization constructed by the simple isotropic material with penalization method, continuous approximation of material distribution, and method of moving asymptotes. Numerical simulations demonstrated that rational and cost effective support layouts can be determined by the proposed cost-based formulation. This allows designers to find design solutions with a compromise between the deformation and the cost of support structure.

Keywords: Additive manufacturing · Support structures · Repulsion index · Topology optimization · SIMP

1 Introduction

Additive manufacturing (AM) becomes the spotlight of the new generation manufacturing processes. Selective laser melting (SLM) is one of the processes and mostly fabricate high added value but low-quantity products by powder bed fusion process, whereas fused deposition modeling (FDM) is widely used for conceptual low-cost rapid prototype development by extrusion-based systems [1–3]. Fabricating overhanging features is one of the efforts in AMs, and two strategies have been proposed to reduce the deformation of overhangs.

The first is modifying the spacemen with self-supporting features that eliminate the need for supports. Leary et al. [4] added extra structures to profiles obtained by topology optimization for self-support during AM. The projection method, proposed by

Gaynor and Guest [5], determined the specimen profiles to ensure that specimen can be manufactured according to the allowing minimum self-supporting angle. Langelaar [6] achieved self-support by constraint aggregation to progressively judge layer-wise accumulation. Hu et al. [7] proposed a method of orientation-driven shape optimization to slim down supports; however, supports were still required at the extreme positions where the specimen surface is convex. Mirzendehdel and Suresh [8] reduced the support volume by the given percentage constraints, and the specimen's geometry varied with different residual percentages. That is, volume constraint percentages 0% implies specimen is self-supporting. The second strategy is to directly add support structures to the overhangs. For eliminating the specimen's surface profile error, adding support structures during AM can restraint warping, fix the specimen on the platform, and improve thermal conduction to prevent internal stress; however, adding supports is time-consuming and dramatically decreases the fabrication efficiency, both of which raise the cost during AM.

Support structures in AM can be classified into internal and external supports. Internal support structures are not only for self-support during the manufacturing process, but also enhance the specimen strength. The external supports are used for self-support and should be removed after the fabrication. This leads to leave artifacts on the specimen and requires further machining effort, which means additional materials and post-processing costs. This study focuses on the external support design with issues such as how supports can be added to improve processing and post-processing efficiency, and how to reduce cost of supports while maintaining specimen geometry regardless of the forces causing the deformation. However, issues regarding AM process parameter optimizations that focus on increasing the product quality are beyond the scope of this study. For instance, numerous unwanted thermo-induced effects such as sagging, balling or time-varying specimen stiffness are not taken into consideration in this study.

The associated costs due to adding supporting structures in the AM process should be taken into consideration in designing the external support, such as the support material amount, the time required to build the support, and the effort to remove it. Various geometrical methods for minimizing the amount of support material were considered analogous to the minimum Steiner tree problem [9–11]. Although geometry-based solutions may minimize the amount of support, the lack of mechanical analysis provides no information regarding the resulting specimen's surface profile error. For example, the forces caused by self-weight. Repetitive cellular or lattice structures are alternatives for minimizing support material consumption [12, 13], and the focus has mostly been the design and generation of the cellular/lattice unit. However, if the purpose of adding supports is to maintain the surface profile error within an acceptable tolerance, the mechanical analysis is a necessity and the finite element analysis is recognized as one of the powerful tools for simulating the AM process. Even though the depicted final support layouts had several discontinuities, trade-off solutions presented by Langelaar [14] provided a compromise between performance and associated cost, which measured printing cost by volume and removal cost by the part-support interface. Buhl [15] expressed the cost as a penalty function to dynamically optimize a layer of support elements as fixed boundary. The support

definition from Buhl is different from that used in AM, but the idea of involving the cost from Buhl in the support topology design is adopt in this study.

In summary, the techniques proposed above [5–8] reduced the material volume of support by varying the specimen's geometry. However, none of these techniques aimed for considering the design requirements such as ease of removal, the fabrication time, and the amount of material used simultaneously. Particularly, the extrusion head traveling time is crucial in FDM fabrication efficiency, yet it hasn't been considered within the support structure optimization. To address these issues, an innovative support structure design strategy based on topology optimization is proposed herein.

This study adopts solid isotropic material with penalization (SIMP) method as material distribution strategy, and continuous approximation of material distribution (CAMD) to avoid checkerboard issue for multiple-objective topology optimization. The design requirements of easy-to-remove, minimization of the cost and surface profile error are expressed as a simple min–max problem and optimized by bound formulation [16–18]. The optimization problem is solved by globally convergent method of moving asymptotes (GCMMA; Svanberg 2007), which has been proven to be an effective large-scale constrained nonlinear optimization solver in recent years. The numerical topology optimization including finite element analysis (FEA) were coded in Matlab.

This article is structured as follows. Section 2 introduces mathematical models that represent easy-to-remove and cost due to time consumption. Section 3 presents numerical examples of structure designs that are easily removed and cost-effective. In this study, we define a distribution force that acts as the trigger for specimen deformation.

2   Requirements for Support Structures in AM Procedures

Adding a support structure during AM is due in great part to reducing deformation caused by the evoked force. The support structure volume should be as less as possible and should also be removed easily while leaving minimal artifacts on the specimen. Moreover, adding a support structure during AM is time-consuming, which reduces the fabrication efficiency. Support structures that use the least amount of material, take least time to add, and can be removed easily are thus the purpose of the optimization.

2.1   The Feature for Easy-to-Remove

Whether the support structure can be easily removed or not is defined by how sparse the support is when it contacts with the specimen. The tinier the contact region of each support, the easier the supports can be stripped from the specimen. Artifacts left on the contact surface can also decrease in certain AM process after stripping. Figure 1a illustrates the contact region in bold white line between the specimen and design domain. The thickness and the number of element layers the contact region consists of can be user defined. A parameter, *repulsion index* (RI), is proposed to make n-th elements $\boldsymbol{\rho}$ in the contact region sparse for easy-to-remove. The layer-wise adjacent condition can be classified as two and three adjacent elements stick together in the contact region of Fig. 1a. For two adjacent elements with densities ρ_1 and ρ_2, ρ_1 feels RI by
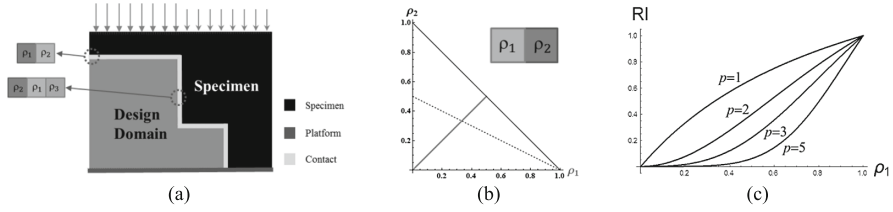
Fig. 1. (a) Contact region between specimen and design domain; (b) Repulsion relationship in 2D finite element model; (c) RI with varying p for $\rho_2 = 1$

$$RI_2(\rho_1) = \frac{\rho_1^p \rho_2^p}{\rho_1^p + \rho_2^p}, \tag{1}$$

where p is a power selected to be equal to the penalty of the density index p in SIMP, and progressively increases from $p = 1$ to $p = 3$ according to continuum method [16]. $RI_2(\rho_1)$ is identified at the intersection between the line through the origin and the line connecting ρ_1 and ρ_2 in Fig. 1b, where $p = 1$. For instance, $RI_2(\rho_1) = 0.5$ if $\rho_1 = \rho_2 = 1$, whereas $RI_2(\rho_1) = 0.33$ when $\rho_1 = 1$ and $\rho_2 = 0.5$ as indicated by the dotted line. Figure 1c shows that RI may behave similarly to the stiffness calculated in the SIMP method under proper choice of p, this property lead the convergence can be smoother during the optimization.

RI experienced by the middle element (ρ_1 in this case) of three adjacent elements illustrated in Fig. 1a can be constructed by several formulations. Three different models to represent $RI_3(\rho_1)$ are introduced in this study. The first is named as "direct three-element"

$$RI_3(\rho_1) = \frac{\rho_1^p \rho_2^p \rho_3^p}{\rho_1^p + \rho_2^p + \rho_3^p}, \tag{2}$$

the second is called "double two-element"

$$RI_3(\rho_1) = \frac{RI_{2L}(\rho_1) RI_{2R}(\rho_1)}{RI_{2L}(\rho_1) + RI_{2R}(\rho_1)}, \tag{3}$$

and the third is "averaged two-element"

$$RI_3(\rho_1) = \frac{RI_{2L}(\rho_1) + RI_{2R}(\rho_1)}{2}, \tag{4}$$

where $RI_{2L}(\rho_1)$ is the RI composed of elements ρ_1 and ρ_2 according to (1), whereas $RI_{2R}(\rho_1)$ consists of elements ρ_1 and ρ_3. The lower the RI is, the sparser the material appears in the contact region.

For applying RI as objective or constraint in gradient-based optimizations like MMA, the sensitivity analysis is required for the numerical calculation iterations. The RI of two elements can be expressed as

$$\frac{\partial RI_2(\rho_{e1})}{\partial \rho_{e1}} = \frac{\partial}{\partial \rho_{e1}}\left(\frac{\rho_{e1}^p \rho_{e2}^p}{\rho_{e1}^p + \rho_{e2}^p}\right) = \frac{\partial}{\partial \rho_{e1}}\left(\frac{\prod_{j=1}^{E}\rho_{ej}^p}{\sum_{j=1}^{E}\rho_{ej}^p}\right) = \frac{p\rho_{e1}^{p-1}\left(\prod_{j=2}^{E}\rho_{ej}^p \sum_{j=1}^{E}\rho_{ej}^p - \prod_{j=1}^{E}\rho_{ej}^p\right)}{\left(\sum_{j=1}^{E}\rho_{ej}^p\right)^2},$$

$$(5)$$

where e indicates the n-th element of the FEA model, j and k represent the subscript index of ρ in Fig. 1a, $\mathbf{\Pi}$ is the product of the sequence of ρ, and E = 2 for two adjacent elements.

By derive (3) as an example, the sensitivity of three elements RI can be expressed as

$$\begin{aligned}\frac{\partial RI_3(\rho_{e1})}{\partial \rho_{e1}} &= \frac{\partial}{\partial \rho_{e1}}\left(\frac{RI_{2L}(\rho_{e1})RI_{2R}(\rho_{e1})}{RI_{2L}(\rho_{e1}) + RI_{2R}(\rho_{e1})}\right) = \frac{\partial}{\partial \rho_{e1}}\left(\frac{\prod_{j=1}^{E}\rho_{Lej}^p \prod_{j=1}^{E}\rho_{Rej}^p}{\prod_{j=1}^{E}\rho_{Lej}^p \sum_{j=1}^{E}\rho_{Rej}^p + \prod_{j=1}^{E}\rho_{Rej}^p \sum_{j=1}^{E}\rho_{Lej}^p}\right)\\ &= \frac{p\rho_{e1}^{p-1}}{(SP(\rho_{e1}))^2}\left[\left(\prod_{j=2}^{E}\rho_{Lej}^p \prod_{j=1}^{E}\rho_{Rej}^p + \prod_{j=1}^{E}\rho_{Lej}^p \prod_{j=2}^{E}\rho_{Rej}^p\right)SP(\rho_{e1})\right.\\ &\quad \left. - \prod_{j=1}^{E}\rho_{Lej}^p \prod_{j=1}^{E}\rho_{Rej}^p\left(\prod_{j=2}^{E}\rho_{Lej}^p \sum_{j=1}^{E}\rho_{Rej}^p + \prod_{j=1}^{E}\rho_{Lej}^p + \prod_{j=2}^{E}\rho_{Rej}^p \sum_{j=1}^{E}\rho_{Lej}^p + \prod_{j=1}^{E}\rho_{Rej}^p\right)\right],\end{aligned}$$

$$(6)$$

and

$$SP(\rho_{e1}) = \prod_{j=1}^{E}\rho_{Lej}^p \sum_{j=1}^{E}\rho_{Rej}^p + \prod_{j=1}^{E}\rho_{Rej}^p \sum_{j=1}^{E}\rho_{Lej}^p, \tag{7}$$

where E = 2, $\rho_{Le1} = \rho_{Re1} = \rho_{e1}$, $\rho_{Le2} = \rho_{e2}$ and $\rho_{Re2} = \rho_{e3}$. Equation (4) than can be similarly derived as (5), and (2) should be derived for E = 3.

2.2 Cost Due to Time Consumption in Adding Support

Adding support structures for overhangs substantially increases the fabrication cost due to amount of material used and the extra time required. Limiting the volume of materials while maximizing the structure stiffness was common in recent structure optimization; however, minimizing the time for building the support remains to be addressed, especially for reducing the extrusion head traveling time in FDM.

When building specimen layer-wised during FDM, the distance between specimen and supports are better to be small for reducing the extrusion head traveling time; thus, this study suggests mapping a series of varying weightings onto the design domain to encourage supports close to the specimen, as illustrated in Fig. 2a. The farther from the specimen, the higher the penalty weighting is. The traveling time of the extrusion head then can be estimated by the user-defined weighting function and the weighting bound. The weighting increases linearly from $w_e = 1$ to $w_{max} = 10$ in this study, and the total cost of the design domain is given by

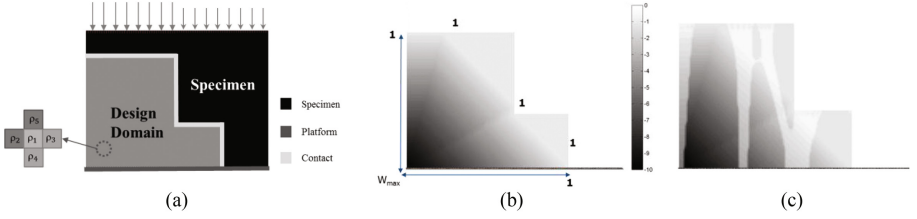$$s(\mathbf{\rho}) = \sum_{e=1}^{N}\rho_e w_e, \tag{8}$$

Fig. 2. (a) Design domain for support material concentration; (b) Linear cost weighting of design domain; (c) Dynamic discount cost weighting of design domain with material concentration considered

where $s(\boldsymbol{\rho})$ is the total cost which can be formulated as either an objective or a constraint, and w_e is the cost weighting corresponding to the element e in the design domain.

Another way to reduce the traveling time is to concentrate the support in a certain region, even though the region is far away from the specimen. For considering the concentration effect, the cost weighting w_e of each element in (8) can be revised for encouraging concentration in terms of RI

$$w_{te} = (1 - p_t RI_w(\rho_e))w_e, \tag{9}$$

where p_t is the support material concentration factor for weighting cost discount, and $RI_w(\rho_e)$ is RI of each element. w_{te} is named as "dynamic discount cost weighting" after the variation support layout during the iterative optimization process. $RI_w(\rho_e)$, which is constructed according to (3), quantifies the repulsion from all adjacent elements in the design domain as depicted in Fig. 2a:

$$RI_w(\rho_1) = \frac{RI_{3H}(\rho_1)RI_{3V}(\rho_1)}{RI_{3H}(\rho_1) + RI_{3V}(\rho_1)}, \tag{10}$$

$$RI_{3H}(\rho_1) = \frac{RI_{2L}(\rho_1)RI_{2R}(\rho_1)}{RI_{2L}(\rho_1) + RI_{2R}(\rho_1)}, \tag{11}$$

$$RI_{3V}(\rho_1) = \frac{RI_{2U}(\rho_1)RI_{2D}(\rho_1)}{RI_{2U}(\rho_1) + RI_{2D}(\rho_1)}, \tag{12}$$

where $RI_{3H}(\rho_1)$ is RI for horizontal elements ρ_1, ρ_2, and ρ_3 and $RI_{3V}(\rho_e)$ is RI for vertical elements ρ_1, ρ_4, and ρ_5. For $w_{max} = 10$ and $p_t = 50\%$, Fig. 2c shows the discount effect from the concentration structure. The reason in formulating $RI_w(\rho_e)$ as (3) instead of (2) or (4) will be discussed in Sect. 3 numerically. The sensitivity of (9) is given by

$$\frac{\partial w_{te}}{\partial \rho_e} = (1 - p_t \frac{\partial RI_w(\rho_e)}{\partial \rho_e})w_e = \left(1 - p_t \frac{\partial}{\partial \rho_e}(\frac{RI_{3H}(\rho_e)RI_{3V}(\rho_e)}{RI_{3H}(\rho_e) + RI_{3V}(\rho_e)})\right)w_e, \tag{13}$$

where

$$\frac{\partial RI_w(\rho_e)}{\partial \rho_e} = \frac{\partial}{\partial \rho_e}\left(\frac{RI_{3H}(\rho_e)RI_{3V}(\rho_e)}{RI_{3H}(\rho_e) + RI_{3V}(\rho_e)}\right) = \frac{\partial}{\partial \rho_e}\left(1 \middle/ \left[\frac{\sum_{j=1}^{E}\rho_{Lej}^p}{\prod_{j=1}^{E}\rho_{Lej}^p} + \frac{\sum_{j=1}^{E}\rho_{Rej}^p}{\prod_{j=1}^{E}\rho_{Rej}^p} + \frac{\sum_{j=1}^{E}\rho_{Uej}^p}{\prod_{j=1}^{E}\rho_{Uej}^p} + \frac{\sum_{j=1}^{E}\rho_{Dej}^p}{\prod_{j=1}^{E}\rho_{Dej}^p}\right]\right).$$

(14)

3 Examples of Easy-to-Remove and Cost-Effective Support Designs

Although the support will be varied for satisfying the three proposed features, the support stiffness still needs to be maintained in certain degree for preserving the specimen profile. A classic support design based on topology structure is demonstrated for assessing the performance of proposed RI and the cost due to additional processing time. Figure 3a and b both depict a uniformly distributed load applied on a beam fixed at both the ends, and the support structure design domain is 0.03 m by 0.04 m and is fixed at the bottom. The initial purpose is only to determine the support structure layout that minimizes the beam deflection. The classic support topology optimization without considering RI and the processing time is formulated as

$$Minimize : \frac{c(\boldsymbol{\rho})}{c_0} = \frac{\mathbf{F}^T\mathbf{u}}{\mathbf{F}^T\mathbf{u}_0} = \frac{\mathbf{u}^T\mathbf{K}\mathbf{u}}{\mathbf{u}_0^T\mathbf{K}\mathbf{u}_0},$$

(15a)

$$Subject\ to : \sum_{e=1}^{N}\rho_e v_e = V \le V_t,$$

(15b)

$$0 < \rho_{\min} \le \rho_e < 1,$$

(15c)

$$\mathbf{K}\mathbf{u} = \mathbf{F},$$

(15d)

where $\mathbf{u}$ is the displacement vector, $\mathbf{F}$ is the force vector, $\mathbf{K}$ is the global stiffness matrix, and subscript 0 in (15a) represents the initial value. $c(\boldsymbol{\rho})$ is the total strain energy of the specimen, where $\boldsymbol{\rho}$ is a N $\times$ 1 vector containing ρ_e, and v_e is the volume
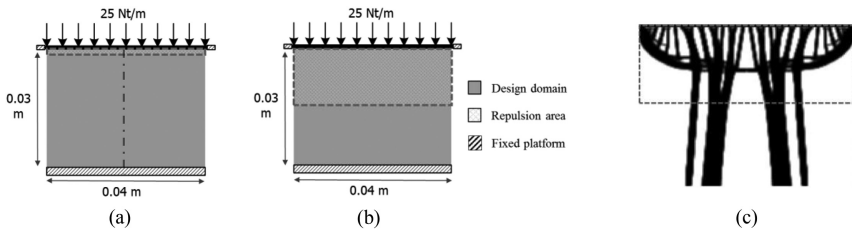

Fig. 3. Topology design for support aiming for easy to remove, (a) 1 mm RI thickness, (b) 14.5 mm RI thickness, and (c) Classic support layout without considering RI and the processing time

of each element; ρ_{min} is a nonzero lower bound of the density (0.0001) which ensures all elements have nonzero stiffness for preventing the singularity while inversing it. Figure 3c illustrates the resulting support topology layout that minimized the compliance while constraining the volume residual at $V_t = 35\%$ of total volume in the design domain.

3.1 Support Structures in Contact Region

Taking the easy-to-remove feature, RI, into consideration, the support topology design expressed in (15a) is rewritten as a multi-objective optimization problem:

$$Minimize : \frac{c(\boldsymbol{\rho})}{c_0} = \frac{\mathbf{F}^T\mathbf{u}}{\mathbf{F}^T\mathbf{u}_0} = \frac{\mathbf{u}^T\mathbf{K}\mathbf{u}}{\mathbf{u}_0^T\mathbf{K}\mathbf{u}_0}, \tag{16a}$$

$$\frac{RI(\boldsymbol{\rho}_r)}{RI_0(\boldsymbol{\rho}_r)} = \frac{RI_2(\boldsymbol{\rho}_2) + RI_3(\boldsymbol{\rho}_3)}{RI_0} \tag{16b}$$

$$Subject\ to : \sum_{e=1}^{N} \rho_e v_e = V \leq V_t, \tag{16c}$$

$$0 < \rho_{\min} \leq \rho_e < 1, \tag{16d}$$

$$\mathbf{K}\mathbf{u} = \mathbf{F}, \tag{16e}$$

where $\boldsymbol{\rho}_2$ and $\boldsymbol{\rho}_3$ represent two and three adjacent elements in the contact region and RI_0 is the initial repulsion index. RI is activated only in part of the design domain circled by the dash line as shown in Fig. 3b. The resulting support topology layouts are respectively illustrated in Fig. 4 for three different RI models described in Sect. 2.1. As can be seen, the double two-element model establishes a support as sparse as it can be in the RI region of Fig. 4b. The phenomenon is not that significant in the other two models as shown in Fig. 4a and c. Comparing $RI_3(\rho_1)$ in the first row of Table 1, values from "direct three-element" and "averaged two-element" both are higher than "double two-element". Even though put all $RI(\boldsymbol{\rho})$ in the same evaluation Eq. (3), double-two element still be the smallest. Therefore, only "double-two element" will be used in the next section for assessing the cost due to processing time.
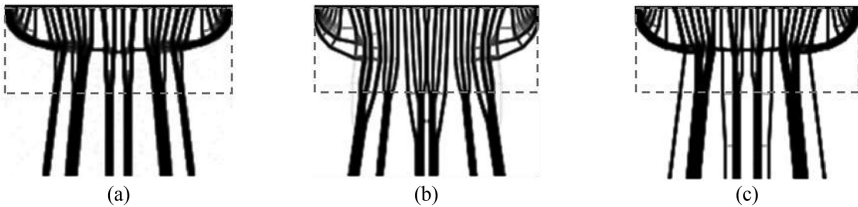

Fig. 4. Support layout with RI included in optimization, (a) direct three-element, (b) double two-element, and (c) averaged two-element

3.2   Minimizing Process Time Due to Adding Support

To take the process time due to adding support into consideration, the optimization described by (16a) is rewritten as

$$Minimize: \frac{c(\boldsymbol{\rho})}{c_0} = \frac{\mathbf{F}^T \mathbf{u}}{\mathbf{F}^T \mathbf{u}_0} = \frac{\mathbf{u}^T \mathbf{K} \mathbf{u}}{\mathbf{u}_0^T \mathbf{K} \mathbf{u}_0}, \tag{17a}$$

$$\frac{RI(\boldsymbol{\rho}_r)}{\mathrm{RI}_0(\boldsymbol{\rho}_r)} = \frac{RI_2(\boldsymbol{\rho}_2) + RI_3(\boldsymbol{\rho}_3)}{\mathrm{RI}_0} \tag{17b}$$

$$\frac{s(\boldsymbol{\rho})}{s_0} = \frac{\sum_{e=1}^{N} \rho_e w_{te}}{s_0} \tag{17c}$$

$$Subject\ to: \sum_{e=1}^{N} \rho_e v_e = V \le \mathrm{V}_t, \tag{17d}$$

$$0 < \rho_{\min} \le \rho_e < 1, \tag{17e}$$

$$\mathbf{K}\mathbf{u} = \mathbf{F}, \tag{17f}$$

where s_0 is the initial cost. Figure 5 illustrate the resulting support layouts according to Fig. 3a after topology optimization using (17a). In the following cases, the initial cost s_0 is assumed to be 35% of the double total cost of Fig. 5d. The total weighting distribution here is symmetrical with the middle vertical line of Fig. 3a; that is, weighting linearly distribute through the design domain for encouraging the materials far from the middle bottom of Fig. 3a. The original cost weighting (i.e., (8) or (9) with $p_t = 0$) of the right-half of Fig. 5a is depicted in Fig. 5d, where the left line of Fig. 5d is the middle of Fig. 3a. The weighting values of the top edge of Fig. 5d are all 1, the value at the left bottom corner is 10, and the value at the right bottom corner is 0. Figure 5b and c represent final profiles from (17) with $p_t = 0.15$ and $p_t = 0.5$ under the same initial weighting distribution as Fig. 5d, and dynamically vary to Fig. 5e and f in the end. Table 2 shows that the cost is lower for higher p_t, and the materials in Fig. 5c are more close to the center in contrast to Fig. 5a and b. The lower compliance and RI ($\boldsymbol{\rho}$) for higher p_t proves that the concentration factor in Fig. 5e and f release the optimization restriction from linear weighting in Fig. 5d. Counting the cost of Fig. 3c with the weighting of Fig. 5d, the final column of Table 2 indicates that minimizing s ($\boldsymbol{\rho}$) remarkably reduced the cost, and $RI(\boldsymbol{\rho})$ also decreased for being objective; however, compliances usually increased for improving the performance of $s(\boldsymbol{\rho})$ and $RI(\boldsymbol{\rho})$ as small as possible.

Table 1. Properties from different $RI_3(\rho_1)$

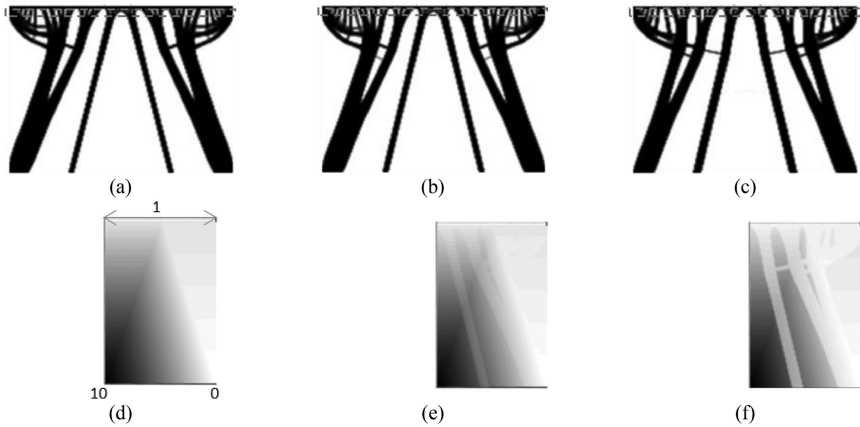| Properties	Direct three elements	Double two elements	Average two elements
$RI(\boldsymbol{\rho})$ with each $RI_3(\rho_1)$	0.41533	0.21059	0.50904
$RI(\boldsymbol{\rho})$ with $RI_3(\rho_1)$ in (3)	0.43511	0.21059	0.41990
Compliance	0.04021	0.04564	0.04075

Fig. 5. Support layout with RI and cost of processing time when (a) $p_t = 0$, (b) $p_t = 0.15$, and (c) $p_t = 0.5$; final weighting distribution with (d) $p_t = 0$, (e) $p_t = 0.15$, and (f) $p_t = 0.5$

Table 2. Properties from different p_t

Properties	$p_t = 0$	$p_t = 0.15$	$p_t = 0.5$	Fig. 3c
$RI(\rho)/RI_0$	0.52578	0.47807	0.47400	0.59834
Cost, $s(\rho)/s_0$	0.20948	0.19715	0.14796	0.39758
Compliance	0.04557	0.04470	0.04249	0.03788

4   Conclusion

This study proposed the RI for support to be easy-removal and the model for quantifying the additional cost due to processing time by adding supports. Both should be included in the topology optimization for external support design in AM. Numerical results show that rational support layouts can be achieved for either easily-removed or cost-effective support structure while maintaining the volume residual percentage. These proposed models can be incorporated into a multi-objective optimization and can be applied to any orientation of the specimen which requires external supports in AM process.

References

1. AM Sub-Platform, European technology Sub-platform in Additive manufacturing, Additive Manufacturing: Strategic Research Agenda (2014). http://www.rm-platform.com/. Accessed 31 June 2016
2. Huang, Y., Leu, M.C., Mazumder, J., Donmez, A.: Additive manufacturing: current state, future potential, gaps and needs, and recommendations. J. Manufact. Sci. Eng. **137**(1), 014001 (2015)
3. Gibson, I., Rosen, D., Stucker, B.: Additive Manufacturing Technologies. Springer, New York (2015)
4. Leary, M., Merli, L., Torti, F., Mazur, M., Brandt, M.: Optimal topology for additive manufacture: A method for enabling additive manufacture of support-free optimal structures. Mater. Des. **63**, 678–690 (2014)
5. Gaynor, A.T., Guest, J.K.: Topology optimization considering overhang constraints: eliminating sacrificial support material in additive manufacturing through design. Struct. Multidiscip. Optim. **54**, 1157–1172 (2016)
6. Langelaar, M.: An additive manufacturing filter for topology optimization of print-ready designs. Struct. Multidiscip. Optim. **55**, 871–883 (2017)
7. Hu, K., Jin, S., Wang, C.C.: Support slimming for single material based additive manufacturing. Comput. Aided Des. **65**, 1–10 (2015)
8. Mirzendehdel, A.M., Suresh, K.: Support structure constrained topology optimization for additive manufacturing. Comput. Aided Des. **81**, 1–13 (2016)
9. Gilbert, E.N., Pollak, H.O.: Steiner minimal trees. SIAM J. Appl. Math. **16**(1), 1–29 (1968)
10. Hwang, F.K., Richards, D.S.: Steiner tree problems. Networks **22**(1), 55–89 (1992)
11. Vanek, J., Galicia, J.A.G., Benes, B.: Clever support: efficient support structure generation for digital fabrication. Comput. Graph. Forum **33**(5), 117–125 (2014)
12. Strano, G., Hao, L., Everson, R.M., Evans, K.E.: A new approach to the design and optimisation of support structures in additive manufacturing. Int. J. Adv. Manufact. Technol. **66**, 1247–1254 (2013)
13. Hussein, A., Hao, L., Yan, C., Everson, R., Young, P.: Advanced lattice support structures for metal additive manufacturing. J. Mater. Process. Technol. **213**(7), 1019–1026 (2013)
14. Langelaar, M.: Topology optimization for additive manufacturing with controllable support structure costs. In: Papadrakakis, M., Papadopoulos, V., Stefanou, G., Plevris, V. (eds.) VII European Congress on Computational Methods in Applied Sciences and Engineering, ECCOMAS, Crete Island, Greece (2016)
15. Buhl, T.: Simultaneous topology optimization of structure and supports. Struct. Multidiscip. Optim. **23**, 336–346 (2002)
16. Bendsøe, M.P., Sigmund, O.: Topology Optimization - Theory, Methods, and Applications. Springer, Heidelberg (2004)
17. Bendsøe, M.P., Sigmund, O.: Topology optimization. In: Arora, S.J. (ed.) Optimization of Structural and Mechanical Systems. World Scientific Publishing Co. Pte. Ltd., pp. 161–194 (2007)
18. Matsui, K., Terada, K.: Continuous approximation of material distribution for topology optimization. Int. J. Numer. Meth. Eng. **59**(14), 1925–1944 (2004)